

Printable anisotropic phantom for EEG with distributed current sources

E. Tsizin* T. Mund† A. Bronstein‡*

August 19, 2018

Abstract

Presented is the phantom mimicking the electromagnetic properties of the human head. The fabrication is based on the additive manufacturing (3d-printing) technology combined with the electrically conductive gel. The novel key features of the phantom are the controllable anisotropic electrical conductivity of the skull and the densely packed actively multiplexed monopolar current sources permitting interpolation of the measured gain function to any dipolar current source position and orientation within the head. The phantom was tested in realistic environment successfully simulating the possible signals from neural activations situated at any depth within the brain as well as EMI and motion artifacts. The proposed design can be readily repeated in any lab having an access to a standard 100 micron precision 3d-printer. The meshes of the phantom are available from the corresponding author.

1 Introduction

Electroencephalography (EEG) is the recording of electrical activity along the scalp, measuring voltage fluctuations resulting from current flows within the neurons of the brain. Being a relatively low cost noninvasive method, EEG has an important role in diagnosis and monitoring of a long list of neurological conditions (with epilepsy being a bold example), and is a valuable tool for brain research [15]. EEG is known to be produced mostly by the synchronous electrical activity of pyramidal neurons. Since these neurons are perpendicular to the human cerebral cortex, EEG is usually modeled as an electrical potential generated by current dipoles perpendicular to the cortex [16]. Reconstruction of neural activity timecourse from EEG is equivalent to the reconstruction of the amplitudes of the current dipoles each representing an activation of a small cortical area. This procedure is called the inverse problem of EEG [8]. While testing a new hardware or an algorithm for the inverse EEG problem solution, it is required to test it

*School of Electrical Engineering, Tel Aviv University

†School of Electrical Engineering, Tel Aviv University

‡Department of Computer Science, Technion – Israel Institute of Technology

in as much realistic environment as possible with known ground truth of sources location and their temporal activity. Studies of this type can be performed using computer simulation (digital phantoms) modeling the propagation of the signal originating within the brain to the electrodes [10]. However, these studies are hardly suited to simulate the motion artifact for the realistic EEG caps (the signals distortion due to the electrodes movement relative to the scalp), electromagnetic interference (EMI) noise generated by the power lines and high power electronic devices [17]. The digital phantoms also cannot be utilized to test new measurement systems. The EEG human studies lack the knowledge of ground truth for the electrical sources location. These limitations of the digital phantoms and human studies provides motivation to the creation of a phantom mimicking the electromagnetic properties of the head and its neural activity.

The electromagnetic properties of the head can be modeled as a volume conductor which consists regions of homogeneous conductivity. Widely accepted is the 3-layer model with the inner layer representing the brain, the middle-the skull, and the outer-the scalp [16]. The brain and the scalp have similar electrical conductivity values while skull is much less conductive. Moreover, the skull's conductivity is anisotropic with the tangential conductivity being about 10 times higher than the radial one. The anisotropy of the human skull influences the signal propagation within the head. Therefore, it influences the accuracy of the inverse problem solution and should be taken into account [25]. With a desired spatial recovery resolution of 1-2cm on the cerebral cortex, the number of possible current sources positions amounts to about 10,000 [16]. An ideal phantom should mimic all these properties and enable activating each one of the possible sources. In addition, the phantom should be reproducible to permit repeating results of any phantom studies in different labs.

A number of phantoms were fabricated. These include the spherical tank filled with saline, gel phantoms, human skulls based and 3d-printed phantoms. The spheres filled with the saline are easy to fabricate but are oversimplified [5]. The human skull based phantoms filled with electrically conductive gel are anatomically correct [12]. However, the skulls are not readily accessible and the results are not fully reproducible as different skulls correspond to different electrical models. The mold making and casting fabrication process was employed to create a phantom with realistic head geometry [4]. The reproducible realistic geometry and varying resistivity head phantom for electrical impedance tomography (EIT) studies was manufactured utilizing 3d-printing technique [14]. There was reported a quasi-anisotropic phantom based on isotropic electrical conductivity layers simulating the anisotropic media [21]. However, no anisotropic phantoms with realistic head geometry are known to the authors except for those based on a real skull. In this phantom type the maximal reported number of 32 current dipoles sources are positioned [12]. No phantoms exist with as many possible sources as the plurality of their meaningful positions.

Presented here is the reproducible 3d-printed realistic head geometry anisotropic phantom which fills the outlined gaps of the existing phantoms. The electrical anisotropy of the skull is achieved by 3d-printing anisotropic texture and filling this texture with the conductive gel. Both the rate of the anisotropy and the conductivity of the skull can be controlled by the parameters of the texture. The plurality of sources aspect of the phantom is achieved by positioning a grid of the quasi-monopolar sources and interpolating/extrapolating the full gain matrix of dipolar current sources in any meaningful

position from a gain matrix of a grid of the monopoles. This interpolation turns to be accurate due to the smoothness of the electrical fields generated by current monopoles and the symmetry of the structure.

The rest of the article is organized as follows: in Section 2 the theory of the EEG forward problem theory is outlined as the basis for the phantom design, in Section 3 the phantom structure and fabrication steps are detailed, in Section 4 the experiment array is explained and the measurements including the gain matrix and EMI measurements are presented, in Section 5 we conclude with implication of our results for the neuroscience community and suggest possible future developments.

2 Theory

Presented here are basics of the EEG forward modeling as this model is at the heart of the phantom design. The changes of neural activity are slow compared to the propagation effects within the biological tissues leading to the quasi-static conditions for the forward EEG problem [18]. The governing equation here is the Poisson equation

$$\nabla \cdot (\sigma \nabla V) = -\nabla \cdot J^p \quad (1)$$

where V is the electric potential, $\sigma(r) \in \mathbb{R}^{3 \times 3}$ is the spatially varying electrical conductivity tensor [10] and J^p is the primary current sources density. The boundary conditions for interfaces with different conductivities are the continuity of the potential V and of the current $\sigma \nabla V$ normal to the interface [10].

The spatial delta current density is called the monopolar current source. Accordingly, the solution of Eq. (1) to such a source is the kernel of the Poisson's operator. In the homogeneous isotropic media (where σ is a position independent scalar), for a monopolar current source with amplitude $I \cdot \delta(r - r_0)$ the resulting potential is given by the following formula:

$$\begin{aligned} \nabla \cdot (\sigma \nabla V) &= I \cdot \delta(r - r_0) \\ V(r) &= \frac{I}{4\pi\sigma |r - r_0|} \end{aligned} \quad (2)$$

Being the simplest possible source, the naïve realization of the monopolar current source is impossible in a system where the electrical charge is conserved. In biological systems the charge conservation usually holds, due to the electrical conductivity of the biological tissue any local accumulation of the electrical charge would result in the compensating electrical currents. The possible realization for the monopolar current source can be achieved by using two equal amplitude and opposite polarity current sources while one of the sources is placed far enough relative to the distance to the observation point (these will be called source and sink of the quasi-monopolar current sources in what follows).

$$\begin{aligned} \nabla \cdot (\sigma \nabla V) &= I \cdot \delta(r - r_0) - I \cdot \delta(r - r_1) \\ V(r) &= \frac{I}{4\pi\sigma |r - r_0|} - \frac{I}{4\pi\sigma |r - r_1|} \approx \frac{I}{4\pi\sigma |r - r_0|}, \quad |r - r_0| \ll |r - r_1| \end{aligned} \quad (3)$$

If the distance between the source and the sink of such a pair is small relative to the distance to the observation point such configuration is called current dipole. The electrical potential it produces is given by the following expression

$$\begin{aligned}
 V(r) &= \frac{I}{4\pi\sigma|r-r_0|} - \frac{I}{4\pi\sigma|r-r_1|} \approx \frac{I \cdot (r_0 - r_1) \cdot (r - \frac{r_0+r_1}{2})}{4\pi\sigma|r - \frac{r_0+r_1}{2}|^3}, \quad |r_1 - r_0| \ll \min(|r - r_1|, |r - r_0|) \\
 V(r) &\approx \frac{I \cdot (r_0 - r_1) \cdot (r - \frac{r_0+r_1}{2})}{4\pi\sigma|r - \frac{r_0+r_1}{2}|^3} = \frac{d \cdot (r - c)}{4\pi\sigma|r - c|^3}, \quad d = I \cdot (r_0 - r_1), \quad c = \frac{r_0+r_1}{2}
 \end{aligned} \tag{4}$$

The quantity $d = I \cdot (r_0 - r_1)$ is defined as the current dipole vector and c is the position of the current dipole. While the electrical potential produced by the current monopole is spherically symmetric, the dipolar source produces potential with a cylindrical symmetry relative to the dipole's axis.

The head consists of biological tissues such as grey and white matter, skull and scalp each having different electrical conductivity. The electrical model consisting of three concentric layers of homogeneous conductivity representing the brain, skull and scalp is widely accepted [10]. A number of studies exist which state some different values for the conductivities of the tissues [7] [9] [11]. The approximate conductivities ranges for the brain, skull and scalp are 0.2-0.9S/m, 0.006-0.015S/m, 0.12-0.6S/m respectively. The ratio between the conductivity of the brain to the conductivity of the skull has major influence on the propagation of the electrical signal from the brain to the scalp. It was estimated from 15 to 80 in different studies [7] [9] [11]. The skull itself consists of a spongiform layer between two hard layers (Figure 1b). Due to higher concentration of ions and water in the spongiform layer it is more electrically conductive than the hard layers. The overall effect of this arrangement is the anisotropic conductivity of the human skull: the tangential conductivity is about 10 times higher than the radial one [20].

The sources of electrical activity are usually modeled as the dipolar current sources perpendicular to the human cerebral cortex. In the human head the quasi-monopolar and dipolar current sources would not induce the same potentials as in the homogeneous media due to the different electrical conductivities of the biological tissues comprising the head. However, the electrical potential of such sources would have some similarity with that induced by the sources in the homogeneous media: the quasi-monopolar current source results in the more isotropic (spherical symmetry) electrical potential distribution while the potential distribution due to dipolar current source has a preferred direction (the dipole direction). The monopolar source in a certain position is determined by a single degree of freedom (its' amplitude) while the dipolar one is determined by two degrees: the amplitude and the direction. This fact will be utilized later in the discussion of the interpolation of the gain matrices produced by the dipolar and monopolar current sources.

While the human brain consists about 10^{11} neurons, meaningful to the EEG studies are approximately 10,000 dipolar sources, each perpendicular to the cortex' convoluted surface [16]. When activated, these dipoles produce electrical potential on the scalp electrodes (EEG). Due to the linearity of the Poisson's equation, the principle of superposition is applied to express the vector of the measured voltages V on the scalp as a

product of the gain matrix G applied to the vector D of the amplitudes of the dipoles:

$$V = GD \quad (5)$$

2.1 The implication of the theory to the phantom design

Mimicking the electromagnetic properties of the head

The method for the implementation of the head's electrical conductivity distribution was inspired by [12] and [2] where the internal volume of a human skull was filled with the conductive gel poured through the pores of the skull and formed by an external container similar to the form of a head mimicking the brain-skull-scalp model. As opposed to a human skull, in this study the skull was 3D-printed (see the fabrication details in the fourth section). The anisotropy of the skull was achieved by printing the layer containing the texture having high percentage of the free volume (the "dipole layer") sandwiched between the layers containing narrow radial tunnels (the "hard layers") and filling these layers with the conductive gel.

The data on electrical conductivity distribution of the skull tissues varies between different studies [7] [9] [11]. While there are studies providing statistical data regarding the geometry of the skull for different ages, races and sexes [1], the authors are unaware of such studies for the electrical conductivity distribution within the skull. Therefore, by printing and testing a phantom with a certain set of electrical parameters the design possesses some universality: the texture parameters can be controlled to implement a range of spatially varying radial and tangential conductivity.

The basic element of the texture is shown on Figure 1. An approximate estimation of the tangential and radial conductivity of this structure can be deduced using the formula for the resistance of the constant cross-section conductor [24]:

$$R = \frac{1}{\sigma} \frac{l}{A} \quad (6)$$

Where R is the resistance, σ is the conductivity of the media, l and A are the length and the cross-section area of the conductor. If only part αA of the cross-section area is conducting with the conductivity σ while the other part is isolator the resistance will be given by

$$R = \frac{1}{\sigma \alpha A} \frac{l}{\alpha A} = \frac{1}{\sigma \alpha} \frac{l}{A} \quad (7)$$

This trivial relationship is showing that in this case the resistance is equal to the resistance of the conductor having cross-section A and the effective conductivity $\alpha\sigma$. This derivation does not take into account the fringing effect of the electrical fields [24] (the current exiting the radial holes is not flowing straight to the opposite radial hole but also in a surrounding volume as in Figure 1). We found that the assumption that the fringing fields are evenly distributed in all the the conductive volume leads to the

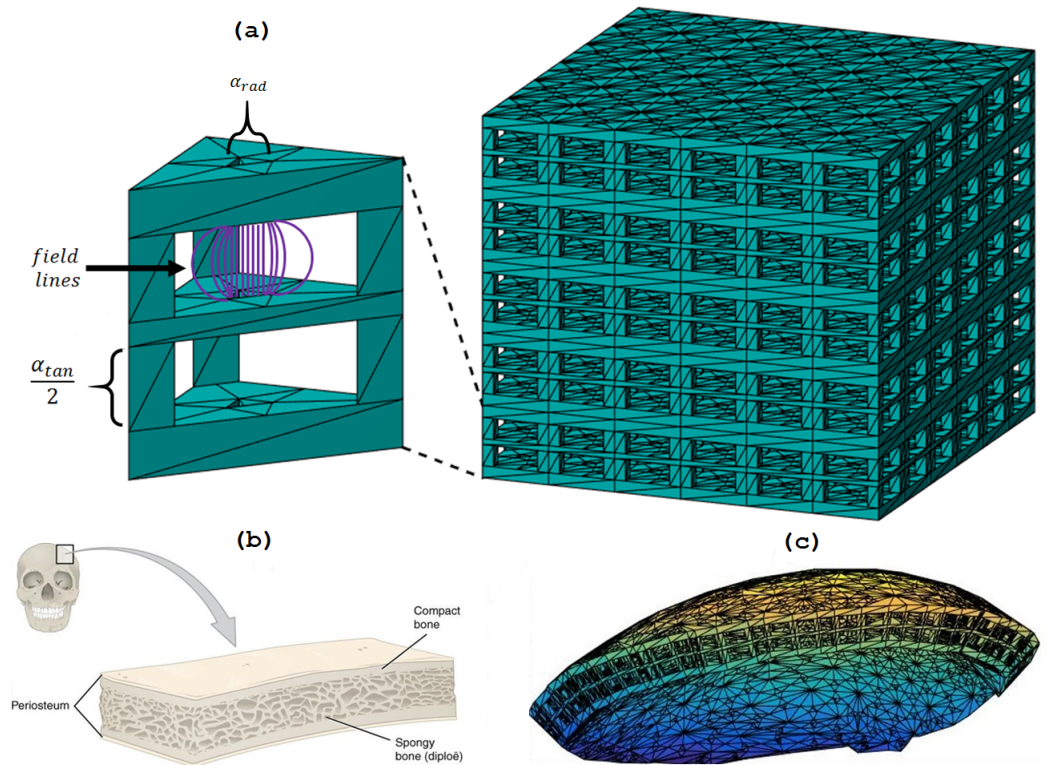


Figure 1: (a) Left: Basic Texture Cell made out of 5 layers: i) 1.5mm layer with a triangular hole. ii) 2.625mm of support pillars. iii) 0.75mm thick layer with a triangular hole. iv) 2.625mm of support pillars. v) 1.5mm layer with a triangular hole. Right: Anisotropic Cube Model. The cubes dimensions is (50,50,45)mm in the corresponding axis. (b) Illustration of general skull structure (c) Sample of the skull with the chosen texture.

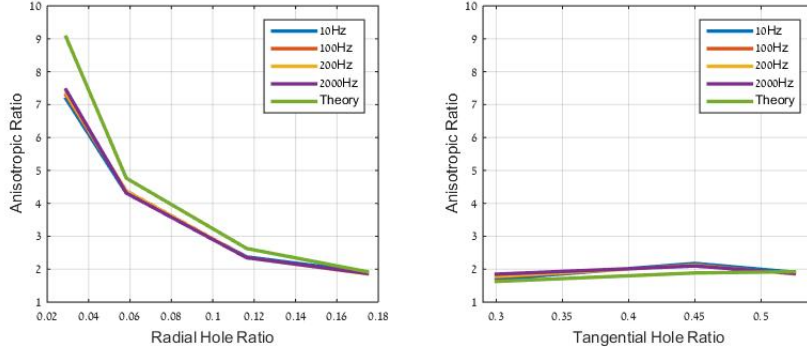


Figure 2: (a) The anisotropic ratio of the 3D printed texture sample is plotted as a function of the radial hole relative area and the tangential hole relative area on the left and right figures respectively. The anisotropic ratio was measured using several frequencies.

theory approximating the real measurements much better than the assumption of the straight field lines.

To estimate the anisotropic ratio based on this theory we assume a solid cube made from an isolating material representing a small part of the skull. The length and the width of the cube are denoted by l while the area of each side by A . The part of the “radial” side area occupied by the holes which are filled then by the conductive gel with conductivity σ is denoted by $A\alpha_{rad}$ and the length part of the “tangential” side occupied by the gap with the supporting pillars which is also filled by the conductive gel is denoted by $l\alpha_{tan}$.

Based on this assumption the resistance of the cube in the vertical direction is calculated as two resistors in series:

$$R_{rad} = \frac{1}{\sigma} \frac{l(1 - \alpha_{tan})}{\alpha_{rad}A} + \frac{1}{\sigma} \frac{l\alpha_{tan}}{A} \quad (8)$$

Where the first argument represents the resistance of the layer with the hole, and the second argument represents the hollow horizontal layer. The resistance of the cube in the horizontal direction is given by:

$$R_{tan} = \frac{1}{\sigma} \frac{l}{\alpha_{tan}A} \quad (9)$$

The anisotropic ratio is given by:

$$\frac{R_{rad}}{R_{tan}} = \frac{(1 - \alpha_{tan}) + \alpha_{tan}\alpha_{rad}}{\frac{\alpha_{rad}}{\alpha_{tan}}} \quad (10)$$

The anisotropic properties of the designed textures was measured and compared to the theoretical formula as can be seen in Figure 2.

Thus by neglecting the influence of the supporting pillars for the tangential conductivity the ratio between the tangential to radial conductivity (the anisotropy) is determined and can be controlled by the size of the radial hole and the thickness of the "diploe" layer. The non-diagonal components of the resulting conductivity tensor are zero since from the construction of the texture element both radial current will not induce tangential potential difference nor the tangential current will induce the radial potential differences as well. The overall effect is that instead of changing the concentration of chemical components for a number of skull pieces controlling the spatially varying electrical conductivity distribution as it was implemented in [14] the parameters of the texture can be controlled for each triangle of the mesh using a computer program. Using this method the gradual tangential and radial conductivity variability can be achieved for different parts of the skull. For the alternating current the capacitive coupling between different conductive parts of the texture filled with the conductive gel (which is similar to the alternating current flowing between the conductive plates of a capacitor separated by the insulating dielectric material) will also influence the conductivity tensor distribution making the simplified formula only approximately correct from one side and introducing another anisotropy controlling parameter of frequency from another (see the Measurements section).

A global tuning parameter of the conductivity distribution within the skull can be the skull width.

We first write the Poisson's equation in Cartesian coordinates

$$\nabla \cdot (\sigma \nabla V) = \nabla \cdot \left(\begin{pmatrix} \sigma_t & 0 & 0 \\ 0 & \sigma_t & 0 \\ 0 & 0 & \sigma_r \end{pmatrix} \begin{pmatrix} \frac{\partial V}{\partial x} \\ \frac{\partial V}{\partial y} \\ \frac{\partial V}{\partial z} \end{pmatrix} \right) = \sigma_t \frac{\partial^2 V}{\partial x^2} + \sigma_t \frac{\partial^2 V}{\partial y^2} + \sigma_r \frac{\partial^2 V}{\partial z^2} \quad (11)$$

We assume the skull width (z-coordinate) was stretched α times. The resulting potential have to obey Poisson's equation

$$z' = \alpha z \quad (12)$$

$$\nabla \cdot (\sigma \nabla V) = \sigma_t \frac{\partial^2 V}{\partial x^2} + \sigma_t \frac{\partial^2 V}{\partial y^2} + \sigma_r \frac{\partial^2 V}{\partial (z')^2} = \sigma_t \frac{\partial^2 V}{\partial x^2} + \sigma_t \frac{\partial^2 V}{\partial y^2} + \frac{\sigma_r}{\alpha^2} \frac{\partial^2 V}{\partial (z)^2} \quad (13)$$

Accordingly the resulting potential distribution is as if in the original coordinates the anisotropy would be α^2 times higher. The "input voltage" on the interface brain-skull would remain approximately the same after changing the skull width since the voltage on this interface is influenced much less than the voltage on the scalp from the decrease of the conductivity of the skull [16]. This property allows us to artificially increase the anisotropy of the skull. Taking typical value of skull thickness 7mm by printing the 9mm skull thickness we both increased the anisotropy value by about 60% and made the structure mechanically more robust. While having a significant influence on the signal propagation through the skull, the change of the skull width by 2mm leaving the scalp width the same and changing its radius by about 2% will have insignificant influence on the signal propagation through the scalp.

The plurality of sources

The wiring of the 10,000 densely packed firmly oriented perpendicular to the cortical surface dipoles within a phantom is technologically challenging. Therefore in all the existing EEG phantoms the small (up to 32 in [12]) representative subset of the dipolar sources was taken.

We choose here another strategy. As the electrical potentials produced by the dipolar sources are smooth and smoothly dependent on the source position we proposed to interpolate the full gain matrix from a gain matrix of a relatively small number of sources. As the sources of neural activity are dipolar it is natural to interpolate the full gain matrix from the gain matrix of the dipolar current sources. As was explained in the previous section, the dipolar current source in a given position is determined not only by its amplitude but also by its orientation. Since the cerebral cortex geometry is highly convoluted, the dipoles perpendicular to it representing the neural activity are changing their orientations significantly on a small spatial scale. Due to the linearity of the forward model, it is possible to interpolate the gain matrix for all the dipole orientations and positions by placing for instance a certain amount of triplets of dipolar sources of linearly independent orientations. Using the gain matrix for these dipoles the interpolant can be deduced for both position and orientation variables of dipolar sources on the cortex. However this way of the gain matrix interpolation is suboptimal. A more elegant and efficient way would be to interpolate the gain matrix using quasi-monopolar sources. As the monopolar source is fully determined by its position and amplitude only a single quasi-monopolar source for each position is required. Placed far enough from the electrodes the sink should be common to all the quasi-monopolar sources. Having the interpolant for the monopolar sources gain matrix the dipolar sources gain matrix can be deduced by interpolating both the gain matrices for the quasi-monopolar sources residing on the cortex and the monopolar sources shifted normally to the cortex by a fixed distance d_0 (for instance 0.1mm) being much smaller than the distance between the sources to the observation points. Since the dipolar source can be represented as the difference of 2 close quasi-monopolar sources having the same sink, the difference of these gain matrices divided by the displacement d_0 results in the dipolar sources gain matrix. Therefore, using the quasi-monopolar sources based gain matrix the number of sources is reduced trifold compared to the dipolar and each source can be a wire and not a pair of closely placed wires with predefined orientation.

In Figure 3 presented is the example of the interpolation error of simulated 64 monopolar sources based gain matrix using natural interpolation/extrapolation to the dipolar cortical sources positions and orientations [19] [13]. The head model we used was an averaged MNI model [6] provided by Brainstorm toolbox [23]. The conductivities of the brain, skull and scalp were taken 0.6S/m, 0.02S/m and 0.6S/m respectively. The common sink of all the quasi-monopolar sources was placed 1cm above the lowest point within the brain region. The electrical potential was measured at 65 vertices of the head mesh corresponding to the standard 10-20 EEG electrodes placement [23]. Since the anisotropy leads to more smooth potentials smearing the electric potential on the skull relative to the isotropic conductivity [25] the simulated interpolation error is an upper bound for the anisotropic case. The gain matrices for both the quasi-monopolar and dipolar sources were calculated using boundary element method (BEM) [22]. For each cortical source k the root mean square (RMS) interpolation error for the gain

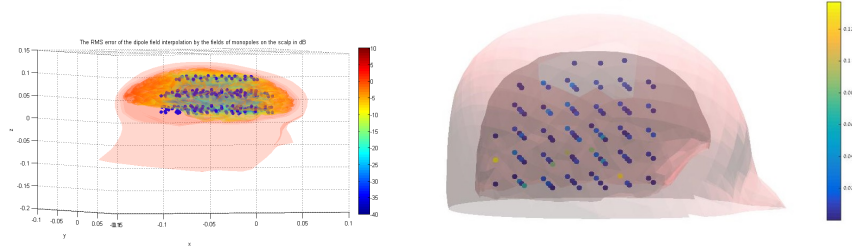


Figure 3: Error visualization. The RMS error for each cortical dipolar source gain vector. (a) Interpolated by the simulated quasi-monopolar sources gain vectors. (b) Interpolated by the true measurements of the quasi-monopolar sources gain vectors using Natural Neighbors Interpolation.

matrix is defined by the following expression

$$\Delta G_k = \frac{\sum_{i=1}^{N_e} (G_{ik} - \bar{G}_{ik})^2}{\sum_{i=1}^{N_e} (G_{ik})^2} \quad (14)$$

where N_e is the number of electrodes, G_{ik} is of the gain matrix value for the dipolar source number k on electrode i and \bar{G}_{ik} is the corresponding element of the interpolated gain matrix.

As expected the interpolation error was smallest for the cortical sources surrounded by the quasi-monopolar ones. The potential for the cortical sources not surrounded by the quasi-monopolar sources was extrapolated and as a consequence was less precise. For the majority of the cortical sources the RMS error was lower than 10%.

3 The phantom structure and fabrication steps

The head phantom was developed according to the following steps: the proper conductivity of the Agar-agar was achieved by dissolving certain amount of salt within the gel. Anisotropic texture was developed and its conductivity tensor was characterized on a simplified cubical models. The mechanical design of the phantom was elaborated. Current sources were positioned inside the phantom. The fabrication process integrating all the design parts was established.

3.1 Materials

Agar-agar was chosen as the conductive material in the phantom. Agar-agar solidifies in room temperature and is stable over time. This property allows the use of the same phantom head for about a month. Salt was used to control the agar's conductivity. For our phantom it was set to $0.67S/m$.

For our physical model and cast we used polylactide(PLA). All head parts were printed using a MakerBot-Replicator2 3d printer.

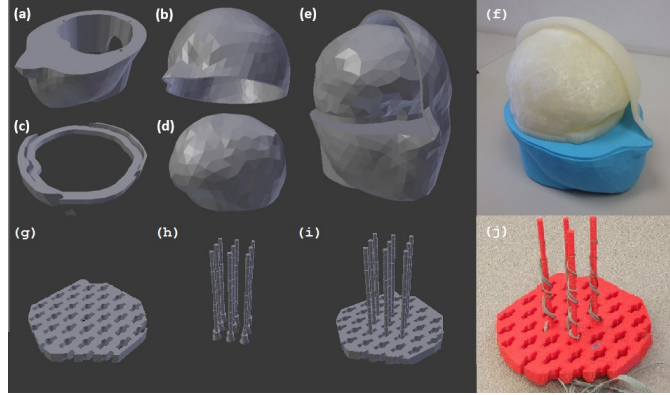


Figure 4: 3D Printed Phantom Parts: (a) Bottom part of the phantom head, with a hole for the sources. (b) Upper head layer, serves as a casting mold. (c) Adapter designed to connect the skull and the head. (d) Smoothed skull. (e) The phantom head model without the right side of the head mold. (f) The 3D-printed model. (g) Base for monopoles poles. (h) Monopole poles. (i) Base with monopole poles. (j) The D-printed monopole structure.

	Brain & Scalp	Skull Radial	Skull Tangential
Conductivity $\frac{S}{m}$	0.667	0.0284	0.207

Table 1: Measured Conductivity Values at 100Hz

3.2 Geometry

The MNI head model provided by Brainstorm toolbox was used as the basis for the head phantom [23]. Triangulated meshes of the inner skull surface and the head were the basis for the phantom geometry. The head triangulated surface was thickened to create a full 3D printable structure of the head, as shown in Figure 4.

3.2.1 Anisotropic Skull Design

Texture samples were synthesized via Matlab. A texture that answers our anisotropic requirements was chosen and imposed upon the skull mesh. Following the triangulated skull mesh, the texture building block was designed as thickened triangle with holes and tunnels as depicted in Figure 1. In order to test its properties, An anisotropic cube model was created by concatenating the basic building blocks in all directions, soaking it in agar solution and testing its conductivity in all three axis. The conductivity values of the agar solution and the skull were measured and can be seen in table 1. The ratio between the vertical conductivity and horizontal conductivity of the cube was 1:7.3 at 100Hz.

In order to impose the texture upon the skull mesh, the following procedure was applied: i) Refining the outer skull mesh ii) Projecting each vertex from the inner mesh

to the outer mesh (finding the closest vertex on the outer mesh) to construct an outer mesh with corresponding vertices. Each face in the outer mesh match a face in the inner mesh. ii) Barycentric coordinates were used to map every vertex in the basic texture cell to the space between matching triangles. The resulting texture can be seen in Figure 1.

3.2.2 Sources Structure

In our design monopolar sources are used. 109 sources are positioned inside the skull. Ground was set at a location as remote as possible from the monopolar sources. 77 sources are densely spread in the right hemisphere and 32 are sparsely spread in the left hemisphere. The density of the sources enables the evaluation of the interpolation error as seen in the next section. A base for support with a Cartesian grid of sockets in which poles can be plugged was designed with a 16.5mm between adjacent sockets in each axis. Each pole is 4mm in diameter and has a series of uniformly spread niches (niche every 15mm). The base and the poles combined enables a 3 dimensional Cartesian grid that can be filled with up to 300 sources. The 3D-printed structure with some sources can be viewed in Figure 4. A calculation showed that the volume the poles occupy in respect to the entire volume of the head is about 1.5%.

3.3 Fabrication Process

In order to combine all of the parts into a complete phantom head model the following steps were taken:

Mold - The right and left parts of the head need to be taped together and securely placed upside down. It is recommended to coat the surface with a simple plastic sheet to shield it from the heat of the liquid solution.

Skull - Superglue was used to attach the skull to the adapter and the adapter to the bottom part of the head. Once the glue solidified, it was placed upside down into the mold.

Sources Structure - Each source is a stripped wire wrapped around a pole. The exposed leftover of the wire is covered with a shrink. Insert the poles into the base. A sample structure can be seen in Figure 4.

Agar - The agar solution is prepared with 32g of agar and 4g of salt per liter of water. 3 liters are enough to fill the phantom. Stir for 20 minutes. Boil it and stir from time to time. Let it cool down to a temperature less than 50 Celsius.

Casting - The agar solution is added slowly until the mold is completely filled. The sources structure is carefully inserted upside down into the hole at the bottom of the skull. At the end, put the whole construction in the fridge until it cools down and solidifies.

4 Experiments

This section focuses on four aspects: The measurement system. The capability of the head phantom to produce desired potential measurements (Calibration). The use of monopolar current sources instead of dipolar ones. The interpolation error of the gain matrix.

4.1 Measurement system

An experimental setup was designed to enable activation of current sources and measurement of scalp potential on the electrodes. A schematic diagram of the setup is shown in Figure 5.

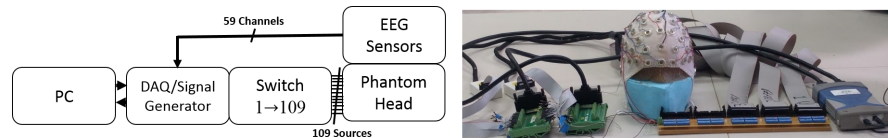


Figure 5: (Left) A schematic diagram of the experiment array. (Right) Experiment array, from right to left: Agilent DAQ Device, Switch, Phantom Head, Analog inputs and Output.

We utilized Agilent U2331A module which integrates a 2-channel signal generator and the 64-channel scope. A mechanical switch multiplex the signal to any current source inside the phantom head. The head phantom wears a 64 electrodes EEG cap produced by EasyCap. Out of the cap's 64 electrodes, 4 are too low to have direct contact with the conductive part of the phantom and 1 is the cheek electrode. The cap is connected to high impedance floating inputs of the measurement device. The DAQ is connected to PC and is operated through Matlab Data Acquisition toolbox. One of the remotely positioned sources is connected to an analog ground of the DAQ and serves as a current sink for all the quasi-monopolar sources within. The entire construct can be seen in Figure 5.

The measurement device, U2331A has a configurable input range and a 12 bit resolution. Due to the linearity of the problem, relatively high current amplitudes were used (0.01-0.05A) to measure the gain matrix with high SNR. The finest voltage resolution that can be captured with the device is $25\mu V$.

4.2 Calibration

For each source, a 100Hz, 5V peak to peak signal was used to activate it. Due to the linearity of the system relative to the input current value of the sources, the amplitude was taken arbitrarily large. The amplitude was limited by the maximal output current of the signal generator. EMI artifacts from the power line which were visible when using low amplitudes(Figure 6) were negligible at this amplitude.

For each source activation the amplitude at the output of each electrode was calculated using a Welch amplitude estimator. The current that was delivered by the device

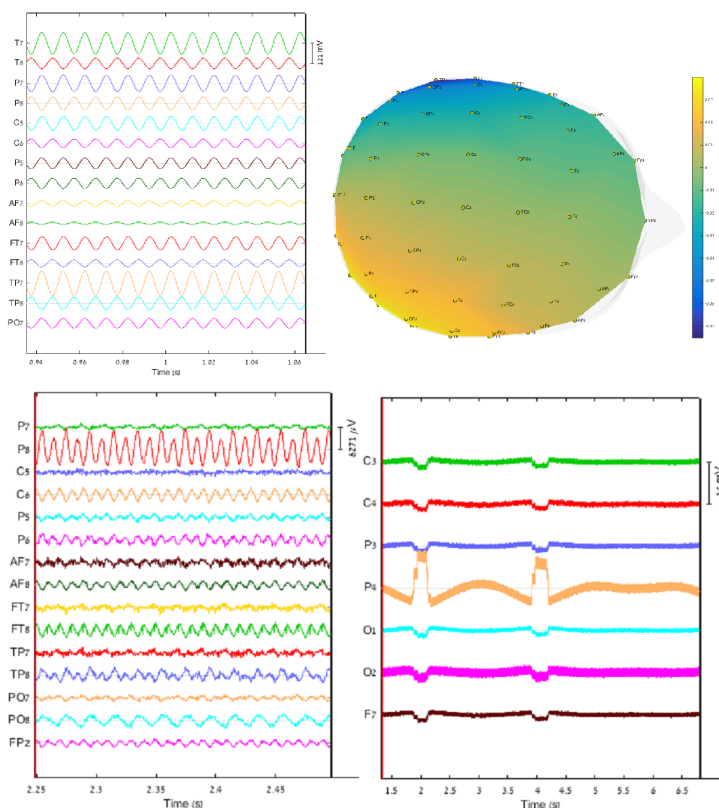


Figure 6: Top row: Sample EEG data waveform and its 2D visualization. Produced by activating a source with a 100Hz sine wave. Bottom row, left: Sample EEG data with visible 50Hz EMI noise. Produced by activating a source using a 100Hz sine wave with a 0.3V amplitude. The phantom head was placed near an electrical device. Bottom row, right: Sample EEG data with visible headset movement.

during each of the activations was measured as well. The phases of the signals were calculated in respect to the current. Each measurement was 20 seconds long. A recording sample is shown in Figure 6.

From the measurements a 59 by 109 gain matrix was obtained.

Regarding the following derivations, we should only mention that we validated the linearity of our system relative to currents for a single frequency of 100Hz.

4.3 Monopoles Justification

Let us denote a dipole activation $d_{i,j}$, as applying 1 unit of current from monopole i to monopole j . In order to retrieve the EEG response to a dipole activation $d_{i,j}$, one can subtract the column g_j of the gain matrix G from the column g_i . In order to verify this quality, 6 couples of monopoles were activated to simulate 6 different

Error	Natural
<i>RMSE</i>	0.0378
<i>MVRE</i>	0.0171

Table 2: Interpolation errors averaged across all monopoles.

dipole activations. The resulting potential per unit of current was compared to the expected potential retrieved by subtracting columns of G . The relative errors between the resulting potential maps were consistently less than 2%.

4.4 Interpolation

For each monopole, two interpolation methods were used to estimate its effect from its neighboring monopoles; Linear interpolation and natural neighbor interpolation [19]. Two error types were used to evaluate the interpolation performance. Let g_i be the true gain column of monopole i in the normalized gain matrix G and \hat{g}_i be the interpolated gain vector. The first error type is Relative Mean Square Error (RMSE) which is defined as follows:

$$RMSE(i) = \frac{\|g_i - \hat{g}_i\|}{\|g_i\|} \quad (15)$$

The second error type is Maximal Value Relative Error(MVRE) which is defined as follows:

$$MVRE(i) = \frac{|g_i(j) - \hat{g}_i(j)|}{|g_i(j)|}, j = \arg \max_k (|g_i(k)|) \quad (16)$$

The average interpolation errors can be seen in table 2. Visualization of the monopoles errors in respect to its position can be seen in Figure 3.

5 Discussion

We successfully designed and fabricated the reproducible phantom for EEG with controllable anisotropy of the skull and the plurality of quasi-monopolar current sources which with reasonable precision can interpolate thousands of meaningful cortical dipolar current sources. While the phantom was designed for EEG it can be adapted to MEG and EIT studies as well. The phantom design possesses universality in controlling the spatial conductivity and anisotropy distribution by texture parameters. While the deduced formula is valid only approximately due to fringing fields, capacitive coupling between conductive regions and the distortion in the current flow introduced by the supporting pillars, it was shown that a calibration step employing the conductivity test on textured cubes filled with conductive gel can be applied to achieve the required conductivity and anisotropy spatial distribution. The change of the anisotropy and the conductivity with frequency can be seen as a sensitivity test of the gain matrix to the change in anisotropy and conductivity distribution. The phantom is designed to multiplex one current source at a time. While simplifying and reducing the cost of the

phantom this possess some limitation on the possibility to activate a number of sources simultaneously. However, in fact this restriction is apparent only: due to the linearity of the problem once the gain matrix (including its frequency response) is measured the signals on electrodes can be calculated for any number of activated sources. Also due to the linearity the influences of EMI, motion artifact [3] or hardware inidealities can be studied with a single source activated and deducing their influence to any number of activated sources. In the presented phantom the skin and the brain volume have the same conductivity. Within the developed methodology the skin volume can be also texturized to reduce its effective conductivity relative to the brain. The brain conductivity is also anisotropic [10]: its volume can be texturized recreating the anisotropic conductivity there making the phantom useful for MREIT and DTI studies as well. These issues we leave for future research.

6 Conclusion

The hardware design for electrophysiological measurement is impossible without being tested properly and reproducibly. EMI and motion artifact can influence the measurements and as a result the quality of the source reconstruction algorithms. Especially susceptible to such artifacts are the so-called dry electrodes which gained recently tremendous popularity for both medical equipment and wearable devices. Here we utilized the flexible and reproducible 3d-printing technique which is penetrating many biological applications to head phantom fabrication. The controllable anisotropy of the skull as well as the plurality of the sources interpolated from current monopoles make this design realistic and easily fabricated. The lifetime of the phantom is about a month - sufficient to support most experimental protocols. The meshes of the phantom are available from the corresponding author. Future research can be focused on the recreation of the electrical conductivity tensor distribution within different organs and on adaptation of the phantom to different imaging modalities such as EIT, MREIT and DTI.

References

- [1] Adelola Adeoye, Kenneth R Kattan, and Frederic N Silverman. Thickness of the normal skull in the american blacks and whites. *American Journal of Physical Anthropology*, 43(1):23–30, 1975.
- [2] S Baillet, G Marin, F Le Rudullier, and L Garnero. γ evoked potentials from a real skull phantom head: An experimental step for the validation of methods for solving the forward & inverse problems of brain cortical imaging. 1997.
- [3] Yu Mike Chi, Tzyy-Ping Jung, and Gert Cauwenberghs. Dry-contact and noncontact biopotential electrodes: Methodological review. *IEEE reviews in biomedical engineering*, 3:106–119, 2010.
- [4] Thomas J Collier, David B Kynor, Jerry Bieszczad, William E Audette, Erik J Kobylarz, and Solomon Gilbert Diamond. Creation of a human head phantom for

- testing of electroencephalography equipment and techniques. *IEEE Transactions on Biomedical Engineering*, 59(9):2628–2634, 2012.
- [5] RJ Cooper, R Eames, J Bruncker, LC Enfield, AP Gibson, and Jeremy C Hebden. A tissue equivalent phantom for simultaneous near-infrared optical tomography and eeg. *Biomedical optics express*, 1(2):425–430, 2010.
- [6] Alan C Evans, D Louis Collins, SR Mills, ED Brown, RL Kelly, and Terry M Peters. 3d statistical neuroanatomical models from 305 mri volumes. In *Nuclear Science Symposium and Medical Imaging Conference, 1993., 1993 IEEE Conference Record.*, pages 1813–1817. IEEE, 1993.
- [7] Sónia I Gonçalves, Jan C de Munck, Jeroen PA Verbunt, Fetsje Bijma, Rob M Heethaar, and F Lopes da Silva. In vivo measurement of the brain and skull resistivities using an eit-based method and realistic models for the head. *IEEE Transactions on Biomedical Engineering*, 50(6):754–767, 2003.
- [8] Roberta Grech, Tracey Cassar, Joseph Muscat, Kenneth P Camilleri, Simon G Fabri, Michalis Zervakis, Petros Xanthopoulos, Vangelis Sakkalis, and Bart Vanrumste. Review on solving the inverse problem in eeg source analysis. *Journal of neuroengineering and rehabilitation*, 5(1):1, 2008.
- [9] David Gutiérrez, Arye Nehorai, and Carlos H Muravchik. Estimating brain conductivities and dipole source signals with eeg arrays. *IEEE transactions on biomedical engineering*, 51(12):2113–2122, 2004.
- [10] Hans Hallez, Bart Vanrumste, Roberta Grech, Joseph Muscat, Wim De Clercq, Anneleen Vergult, Yves D’Asseler, Kenneth P Camilleri, Simon G Fabri, Sabine Van Huffel, et al. Review on solving the forward problem in eeg source analysis. *Journal of neuroengineering and rehabilitation*, 4(1):1, 2007.
- [11] Y Lai, W Van Dronghen, L Ding, KE Hecox, VL Towle, DM Frim, and B He. Estimation of in vivo human brain-to-skull conductivity ratio from simultaneous extra-and intra-cranial electrical potential recordings. *Clinical neurophysiology*, 116(2):456–465, 2005.
- [12] RM Leahy, JC Mosher, ME Spencer, MX Huang, and JD Lewine. A study of dipole localization accuracy for meg and eeg using a human skull phantom. *Electroencephalography and clinical neurophysiology*, 107(2):159–173, 1998.
- [13] Hugo Ledoux and Christopher Gold. An efficient natural neighbour interpolation algorithm for geoscientific modelling. In *Developments in spatial data handling*, pages 97–108. Springer, 2005.
- [14] Jian-Bo Li, Chi Tang, Meng Dai, Geng Liu, Xue-Tao Shi, Bin Yang, Can-Hua Xu, Feng Fu, Fu-Sheng You, Meng-Xing Tang, et al. A new head phantom with realistic shape and spatially varying skull resistivity distribution. *IEEE Transactions on Biomedical Engineering*, 61(2):254–263, 2014.

- [15] Ernst Niedermeyer and FH Lopes da Silva. *Electroencephalography: basic principles, clinical applications, and related fields*. Lippincott Williams & Wilkins, 2005.
- [16] Paul L Nunez and Ramesh Srinivasan. *Electric fields of the brain: the neurophysics of EEG*. Oxford University Press, USA, 2006.
- [17] Anderson S Oliveira, Bryan R Schlink, W David Hairston, Peter König, and Daniel P Ferris. Induction and separation of motion artifacts in eeg data using a mobile phantom head device. *Journal of neural engineering*, 13(3):036014, 2016.
- [18] Robert Plonsey and Dennis B Heppner. Considerations of quasi-stationarity in electrophysiological systems. *The Bulletin of mathematical biophysics*, 29(4):657–664, 1967.
- [19] Sibson R. A brief description of natural neighbour interpolation. In *Interpreting multivariate data* (Ed. Barnett V.), pages 21–36, 1981.
- [20] Stanley Rush and Daniel A Driscoll. Current distribution in the brain from surface electrodes. *Anesthesia & Analgesia*, 47(6):717–723, 1968.
- [21] Rosalind J Sadleir, Farida Neralwala, Tang Te, and Aaron Tucker. A controllably anisotropic conductivity or diffusion phantom constructed from isotropic layers. *Annals of biomedical engineering*, 37(12):2522–2531, 2009.
- [22] Matti Stenroos, Ville Mäntynen, and Jukka Nenonen. A matlab library for solving quasi-static volume conduction problems using the boundary element method. *Computer methods and programs in biomedicine*, 88(3):256–263, 2007.
- [23] François Tadel, Sylvain Baillet, John C Mosher, Dimitrios Pantazis, and Richard M Leahy. Brainstorm: a user-friendly application for meg/eeg analysis. *Computational intelligence and neuroscience*, 2011:8, 2011.
- [24] Jack Vanderlinde. *Classical electromagnetic theory*, volume 145. Springer Science & Business Media, 2006.
- [25] Carsten Hermann Wolters, Alfred Anwander, Xavier Tricoche, D Weinstein, Martin A Koch, and Robert S Macleod. Influence of tissue conductivity anisotropy on eeg/meg field and return current computation in a realistic head model: a simulation and visualization study using high-resolution finite element modeling. *NeuroImage*, 30(3):813–826, 2006.